Oxygen Mass Transport Limitations at the Cathode of Polymer Electrolyte Membrane Fuel Cells

Jay Benziger, Erin Kimball, Raquel Mejia-Ariza, and Ioannis Kevrekidis
Dept. of Chemical Engineering, Princeton University, Princeton, NJ 08544

DOI 10.1002/aic.12455
Published online December 3, 2010 in Wiley Online Library (wileyonlinelibrary.com).

Oxygen transport across the cathode gas diffusion layer (GDL) in polymer electrolyte membrane (PEM) fuel cells was examined by varying the O_2/N_2 ratio and by varying the area of the GDL extending laterally from the gas flow channel under the bipolar plate (under the land). As the cathode is depleted of oxygen, the current density becomes limited by oxygen transport across the GDL. Oxygen depletion from O_2/N_2 mixtures limits catalyst utilization, especially under the land.The local current density with air fed PEM fuel cells falls to practically zero at lateral distances under the land more than 3 times the GDL thickness; on the other hand, catalyst utilization was not limited when the fuel cell cathode was fed with 100% oxygen. The ratio of GDL thickness to the extent of the land is thus critical to the effective utilization of the catalyst in an air fed PEM fuel cell.
 AIChE J, 57: 2505–2517, 2011
Keywords: PEM fuel cell, mass transport limited current, gas diffusion layer

Introduction

Polymer electrolyte membrane (PEM) fuel cells are electrochemical cells that oxidize hydrogen to produce an electrical current through an external load resistance. Figure 1 is a schematic of a PEM fuel cell. Reactant gases are fed through flow channels machined in bipolar plates. The bipolar plates are pressed against a membrane-electrode-assembly (MEA). The MEA consists of five principal layers: (i) a polymer electrolyte which conducts protons; (ii, iii) catalyst layers coated onto both sides of the electrolyte membrane, forming the anode and cathode; and (iv, v) porous conducting layers [the gas diffusion layer (GDL)] which conduct the electronic current and permit reactants to get from the gas flow channels to the catalyst layers. The bipolar plate contacts the GDL to carry the current through the external circuit. The area where the bipolar plate is in direct contact with the GDL is known as the land, or the rib. At both electrodes, the reactant gases must be transported from the gas flow channels through the GDL to the catalyst layers where the electrochemical reactions occur. When operating a PEM fuel cell with hydrogen and oxygen, the gas composition in the flow channels remains nearly constant throughout the fuel cell (consumption of reactants reduces the gas flow rates but does not alter the compositions). When air is employed as the oxygen source at the cathode, oxygen is consumed by the reaction and the concentration of oxygen is reduced between the inlet and outlet of the cathode gas flow channels. The driving force for oxygen transport from the flow channel to the catalyst/PEM interface is diminished as the oxygen concentration decreases.

The current through the load resistance depends on the sequence of transport and chemical reaction steps summarized below.[1,2]

Transport and reaction steps in PEM fuel cells

(1) Hydrogen is fed to the anode flow channel.
(2) Hydrogen transport through the anode GDL from the anode gas flow channel to the anode catalyst layer.

Correspondence concerning this article should be addressed to J. Benziger at benziger@princeton.edu.

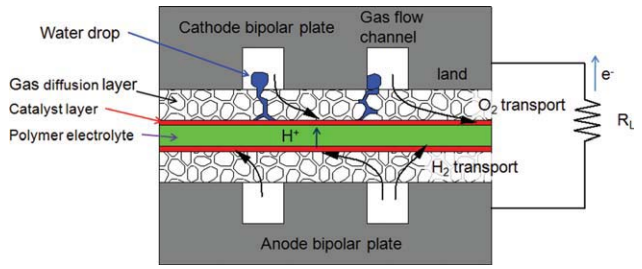

Figure 1. Schematic of transport in a PEM fuel cell.

Oxygen and hydrogen flow through gas flow channels in the bipolar plates at the cathode and anode, respectively. The O_2 and H_2 must be transported through the gas diffusion layers to the respective catalyst layers where the electrochemical reactions occur. [Color figure can be viewed in the online issue, which is available at wileyonlinelibrary.com.]

(3) Hydrogen oxidation to protons and electrons at the anode catalyst layer.

(4) Proton transport through the PEM from the anode catalyst layer to the cathode catalyst layer. (Proton transport is in parallel to electron transport through the external load resistance from the anode catalyst layer to the cathode catalyst layer).

(5) Oxygen (or air) is fed to the cathode flow channel.

(6) Oxygen transport through the cathode GDL from the cathode gas flow channel to the cathode catalyst layer.

(7) Oxygen reduction to water at the cathode catalyst layer.

At steady state all seven steps proceed at the same rate, but often one step in the sequence is rate limiting, when the rate coefficient for that step (e.g., reaction rate constant, diffusion coefficient or membrane ionic resistance) is much less than the rate coefficients for the other steps. With fuel cells three different rate limiting steps are generally identified based on the dependence of the voltage across the load resistance on the current through the load resistance.

Activation Regime. Reaction kinetics at the cathode or anode catalysts is rate limiting. The voltage drops rapidly with current density and then levels out $\left(\frac{\partial V}{\partial I}<<0,\ \frac{\partial^2 V}{\partial I^2}>0\right)$. The activation regime is at low current density (or large load resistance). The voltage drops from the thermodynamic potential by the activation potential drop, η_{act}, which corresponds to the activation energy for the rate limiting electrode reaction.

Ohmic Regime. Resistance to current flow across the PEM is the rate limiting step. This is normally identified as the region at intermediate current density, where the voltage decreases linearly with current. $\left(\left(\frac{\partial V}{\partial I}\right)_{\text{ohmic}}=-R_{\text{membrane}}\right)$.

Mass Transport Regime. Mass transport of a reactant from the gas flow channel to the catalyst layer limits the current and the voltage decreases rapidly to zero at a limiting current density. $\left(\left(\frac{\partial V}{\partial I}\right)_{\substack{\text{mass}\\ \text{transport}}}\rightarrow-\infty\right)$.

Mass transport limitations are generally attributed to diffusional resistances across the GDL. The GDL is a porous electronic conductor that permits transport of gases to the catalyst/PEM interface and transport of liquid water to the gas flow channels. Liquid water in the GDL is frequently assumed to be the major cause of mass transport limitations.[3–5] Our group has shown that hydrophobic porous carbons with a bimodal pore size distribution push product liquid water from the catalyst layer to the gas flow channel through the largest pores of the hydrophobic GDL at the cathode, leaving most of the small pores available to transport gas from the gas flow channel to the catalyst/PEM interface.[6,7] Other groups have confirmed that the amount of water in the GDL is small even in the mass transport limited regime of PEM fuel cell operation.[8–10]

The distance for gas transport through the GDL can result in low utilization of catalyst. Reactants must be transported from the flow channel to the electrode/membrane interface, and the increased transport distance under the land may cause part of the electrode to be in a mass transport limited regime. Several investigators have employed 2D and 3D models to show that at low output voltage (high current density) the local current density is less under the land than under the gas flow channel.[11–16]

Mass transport limitations from standard fuel cell test stations with serpentine and parallel flow channels, which give an integral current output and average voltage, are difficult to quantify. We report here quantitative measurements of mass transport obtained with the one-dimensional stirred tank reactor (STR) PEM fuel cell and two-dimensional parallel flow channel (PFC) PEM fuel cells. Details of these fuel cells can be found in the literature.[17,18] The STR PEM fuel cell replaces the flow channels with an open plenum, where the convective velocity is low and gas phase diffusion is sufficient to mix the gas uniformly. The STR PEM fuel cell permits a simple correlation of the oxygen concentration at the cathode with the current density. The PFC PEM fuel cell has a single flow channel at each of the anode and cathode. It was possible to vary the ratio of the width of the flow channel to the width of the MEA, thus altering the distance for transport from the flow channel to the catalyst under the land, which in turn affects catalyst utilization. Results with these model fuel cells show that the dilution of oxygen by nitrogen in the air causes mass transport limitations that can lead to poor catalyst utilization if the channel to land area ratio is small.

Experimental

An STR PEM fuel cell was employed to study the role of cathode gas composition on mass transport limitations. The design of the fuel cell system and MEA fabrication is described elsewhere.[17] Briefly, the fuel cell operated as a 1-dimensional system with an MEA area of $\sim$1.8 cm^2 and gas volumes at the anode and cathode of 0.36 cm^3. The MEAs were made with Nafion 115 membranes and ETEK electrodes; a Pt/C catalyst layer was hot-pressed onto the membrane. The ETEK electrodes were carbon cloth GDL $\sim$0.4 mm thick with a thin, $\sim$0.02 mm, thick microporous catalyst layer.

The STR PEM fuel cell

The STR PEM fuel cell was operated at 1 bar pressure (both anode and cathode). The fuel cell was run autohumidified (dry feeds were employed). It has been demonstrated that the autohumidified PEM fuel cell gives identical current/voltage output as a fuel cell with humidified feeds as long as the fuel cell is operated above the critical threshold

current for current ignition.[19] The anode was fed with pure hydrogen at 8 sccm, (3.0×10^{-6} m/cm^2 s = 0.58 amp-H$^+$/cm^2). The cathode was fed with a mixture of O_2 and N_2.Feeds of O_2 and N_2 were metered through separate mass flow controllers with a total flow rate of 8 sccm. The inlet compositions were varied from 0 to 100% O_2. The fuel cell was heated by cartridge heaters and the tests were done at 25, 45, 60 and 80°C.

Reproducible MEA conditions for all the tests were achieved by operating the fuel cell under galvanostatic control at the specified temperature for 1 hour, at a total current of 0.5 A (0.28 A/cm^2) with feeds of 8 sccm of hydrogen at the anode and 8 sccm of oxygen at the cathode; this was sufficient to have the membrane fully humidified (via autohumidification). After 1 hr, the internal resistance was measured by current interrupt. The cathode feed O_2/N_2 ratio was adjusted; the fuel cell was put under potentiostatic control at a voltage of 0.95 V and allowed to equilibrate for 2 minutes (to refresh the gas composition at the anode and cathode). The current was recorded while the voltage was stepped from 0.95–0.025 V at a rate of 0.0125 V/s by an Arbin data acquisition system (DAQ) running the Arbin's MSTAT4+ software. After completing the IV sweep the internal resistance was again recorded and the fuel cell restored to galvanostatic control. The IV curve was swept in <2 minutes and the membrane resistance changed by <5% between before the voltage sweep and after the voltage sweep. The negligible change in the membrane resistivity indicated that the water content remained nearly constant during the test. Our group has also measured water desorption rates from Nafion into dry nitrogen; at $T \leq 90$°C the maximum water loss in the 4 minutes of the test if there were no water produced would be <30%.[20,21] The resistance measured by current interrupt is less than the resistance determined from the slope of the IV curve. The current interrupt method measures the resistance in the membrane but does not capture the interfacial resistance in the catalyst layer, so it represents a low estimate of the internal resistance of the fuel cell.

The PFC fuel cell

The PFC fuel cell was used to study the lateral transport of reactants by changing the width of the MEA under the lands. A schematic of the cross section of one side of the fuel cell is shown in Figure 2. The width of the MEA was varied from 4.8 mm (3/16″; 1.6 mm under the channel and 1.6 mm under each land) to 14.3 mm (9/16″; 1.6 mm under the channel and 6.4 mm under each land). The axial current profile and total current were recorded for fixed external load resistance.

Experiments were conducted to compare the current obtained with a pure O_2 feed and with an air feed; the fuel cell was oriented vertically with cocurrent feeds from the top (this configuration facilitates gravity draining of the liquid water formed at the cathode). All the experiments with the PFC fuel cell were performed at room temperature, so the water vapor pressure was low and made up a negligible fraction of the gas composition at both the anode and cathode. The fuel cell was operated autohumidified with dry feeds. Relative humidity sensors at the outlets of the anode and cathode showed that effluents were fully humidified for all operating conditions.

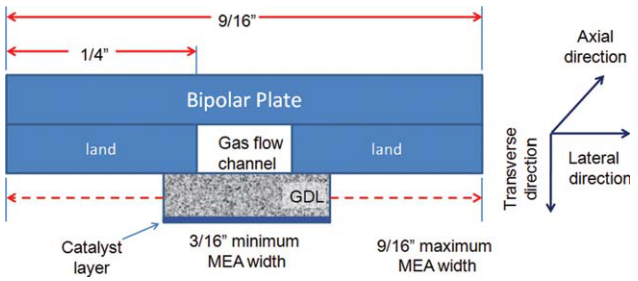

Figure 2. Schematic of the cross-section of the PFC fuel cell showing the variation in the path-length through the GDL with different widths of MEA.

The width of the MEA is increased from 4.8 mm (3/16″; 1/16″ under the channel and 1/16″ under each land) to 14.3 mm (9/16″; 1/16″ under the channel and 1/4″ under each land). [Color figure can be viewed in the online issue, which is available at wileyonlinelibrary.com.]

The MEAs used in the PFC fuel cell were made by hot pressing Pt/C catalyst single sided ETEK electrodes onto both sides of a Nafion 115 membrane. The MEAs were 6.1 cm long with widths that varied from 4.8 to 14.3 mm. The fuel cell was always operated with a 2:1 hydrogen/oxygen stoichiometry. It was started with low flows of 6/3 sccm H_2/O_2, or 6/14.3 sccm H_2/air, for one hour (''Startup''). After 1 hr the flow rates were increased to a stoichiometric excess of reactants of ~100% ($F_{H_2}^{feed} = 2 \times (i/2\boldsymbol{F})$; $F_{O_2}^{feed} = 2 \times (i/4\boldsymbol{F})$). The anode flow was always 12 sccm H_2. The cathode flow was 6 sccm O_2or 28.6 sccm air. After 2 hrs the H_2/O_2 feeds were reduced until no gas was detected leaving the fuel cell—these flow rates were approximately 6 sccm of H_2 and 3 sccm O_2. The current was then measured as a function of the MEA width with fixed load impedance. The ratio of the pressure drop along the length of the flow channel to the total pressure was estimated assuming laminar flow through a straight channel ($\Delta P/P = \{8\mu L_{channel}\ F^{feed}/RT\}/R_H^4$). The ratio was 10^{-3} indicating that the pressure could be considered to be uniform along the length of the flow channel.

Results

Current density compositional dependence

IV data from the STR PEM fuel cell with different cathode feed compositions at 45°C are shown in Figure 3 (similar data was obtained at 25, 60, and 80°C).Three ''polarization'' regimes are evident in the data: (1) activation polarization at low current densities less than 0.1 A; (2) ohmic polarization in the moderate current range, approximately 0.1–1 A; and (3) mass transport polarization where $\left(\frac{\partial V}{\partial I}\right) \rightarrow -\infty$.

The IV curves are shifted downward with decreasing oxygen mole fraction in the cathode feed. A small downward shift is to be expected from thermodynamics; the voltage change associated with a change in oxygen partial pressure can be described by the Nernst equation based on the gas compositions in the flow channels (Eq. 2, later).

The STR PEM fuel cell has spatially uniform gas composition in the gas flow channel. The mass balance gives the mole fraction of oxygen at the cathode (Eq. 1).

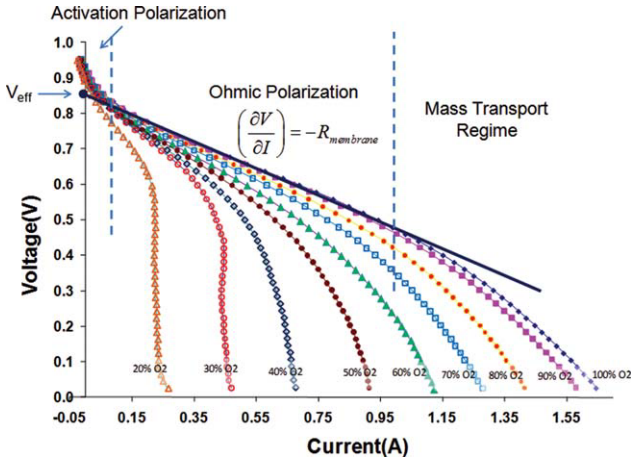

Figure 3. IV curves for the STR PEM fuel cell as a function of the cathode feed composition.

Data shown are for operation at 45°C, with feeds of 8 sccm H_2 at the anode and 8 sccm (O_2+N_2) at the cathode; the percentage of oxygen in the cathode feed is noted. Approximate dividing lines between different rate limiting steps with 100% O_2 feed have been drawn. [Color figure can be viewed in the online issue, which is available at wiley onlinelibrary.com.]

$$x_{O_2}^{\text{cathode}} = \frac{F_{O_2} - \frac{i}{4F}}{\left(F_{O_2} + F_{N_2} - \frac{i}{4F}\right)\left(\frac{P_T}{P_T - P^0_{H_2O}}\right)} \tag{1}$$

The hydrogen pressure at the anode was the same for all the experiments. The cathode gas stream was always saturated with water (per RH sensor readings), so the water vapor activity at the cathode was always unity, independent of nitrogen mole fraction. At fixed temperature only the oxygen mole fraction at the cathode was different when changing from 100% O_2 feed to an O_2/N_2 mixture at the same temperature. If the gas composition at the catalyst layer is equal to that in the cathode gas flow channel the thermodynamic shift of the IV curve between an O_2 feed and an O_2+N_2 feed is only dependent on the ratio of the oxygen mole fractions, as expressed in Eq. 2. Figure 4 compares the experimental data of a 100% O_2 feed and a 50/50 N_2/O_2 feed at 45°C, along with thermodynamic correction of the IV curve from 100% O_2 feed to a 50/50 N_2/O_2 feed, based on Eq. 2.

$$\Delta V = \frac{RT}{2F}\ln\frac{P_{H_2}^{\text{anode}}\left(P_{O_2}^{\text{cathode}_{\text{oxygen}}}\right)^{1/2}}{P_{H_2O}^{\text{cathode}}} - \frac{RT}{2F}\ln\frac{P_{H_2}^{\text{anode}}\left(P_{O_2}^{\text{cathode}_{O_2+N_2}}\right)^{1/2}}{P_{H_2O}^{\text{cathode}}} = \frac{RT}{2F}\ln\frac{\left(x_{O_2}^{\text{cathode}_{O_2+N_2}}\right)^{1/2}}{\left(x_{O_2}^{\text{cathode oxygen}}\right)^{1/2}} \tag{2}$$

The predicted downward shifts of the IV curves between O_2 and O_2/N_2 mixtures are ~10 mV while the experimental results showed downward shifts of >100 mV. The internal resistance, before and after every IV sweep was nearly constant, $R_m = 0.43 \pm 0.03\ \Omega$. We suggest that most of the reduction in voltage at fixed current when changing from O_2 to O_2+N_2 mixtures is the result of oxygen mass transport resistance across the GDL.

To understand the mass transport resistance we seek to identify how the current depends on oxygen mole fraction in the cathode gas flow channel at constant load impedance. The load resistance is the independent system parameter that is varied in obtaining the IV curves. At every data point from Figure 3 compositions in the gas flow channels at the anode and cathode were determined from mass balances given by Eqs. 3 and 4, and the load resistance can be determined from the ratio of V/I.

$$x_{H_2O}^{\text{anode}} = \frac{P^0_{H_2O}}{P_T}$$
$$x_{H_2}^{\text{anode}_{\text{channel}}} = 1 - \frac{P^0_{H_2O}}{P_T} \tag{3}$$

$$x_{H_2O}^{\text{cathode}} = \frac{P^0_{H_2O}}{P_T}$$
$$x_{N_2}^{\text{cathode}_{\text{channel}}} = \frac{x_{N_2}^{\text{in}}\left(1 - \frac{P^0_{H_2O}}{P_T}\right)}{1 - \frac{i}{4F\left(F_{O_2+N_2}^{\text{cathode}}\right)}} \tag{4}$$
$$x_{O_2}^{\text{cathode}_{\text{channel}}} = \frac{\left(x_{O_2}^{\text{in}} - \frac{i}{4F\left(F_{O_2+N_2}^{\text{cathode}}\right)}\right)\left(1 - \frac{P^0_{H_2O}}{P_T}\right)}{1 - \frac{i}{4F\left(F_{O_2+N_2}^{\text{cathode}}\right)}}$$

Current as a function of gas phase composition at fixed load resistance is shown in Figure 5. The current increased linearly with oxygen mole fraction and then asymptoted to a value dependent on load resistance. The linear increase of current with oxygen mole fraction at low mole fraction is indicative of oxygen mass transport from the cathode gas flow channel to the catalyst/membrane limiting the current. When the current plateaued at higher oxygen mole fraction, it was limited by the load resistance. The transition between

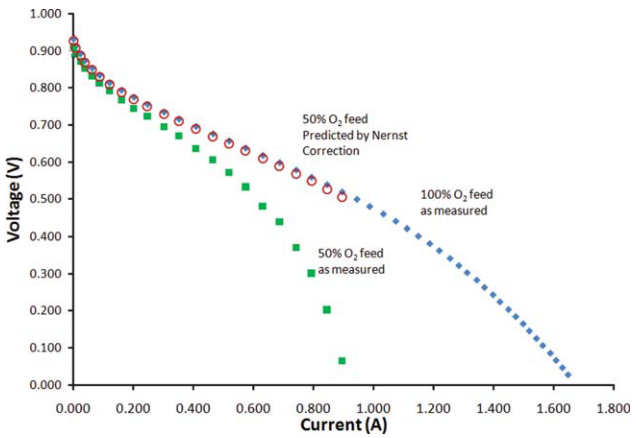

Figure 4. A comparison of the IV curves for 100% O_2 feed (solid diamonds), 50% O_2/50% N_2 (solid squares), and the IV curve for 50% O_2/50% N_2 predicted using the oxygen mole fraction in the cathode channel relative to 100% O_2 in the cathode channel (open circles).

[Color figure can be viewed in the online issue, which is available at wileyonlinelibrary.com.]

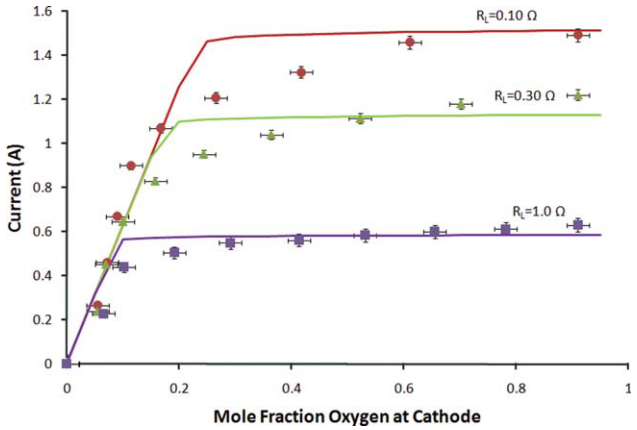

Figure 5. Current as a function of oxygen mole fraction in the cathode gas flow channel in a STR PEM fuel cell at different load impedances.

These data were extracted from Figure 3. The mole fraction at the cathode was evaluated using Eq. 2. The resistance of the membrane in the fuel cell was 0.23 Ω, determined from current interrupt measurements.The solid lines are model predictions based on Eq. 6. [Color figure can be viewed in the online issue, which is available at wileyonlinelibrary.com.]

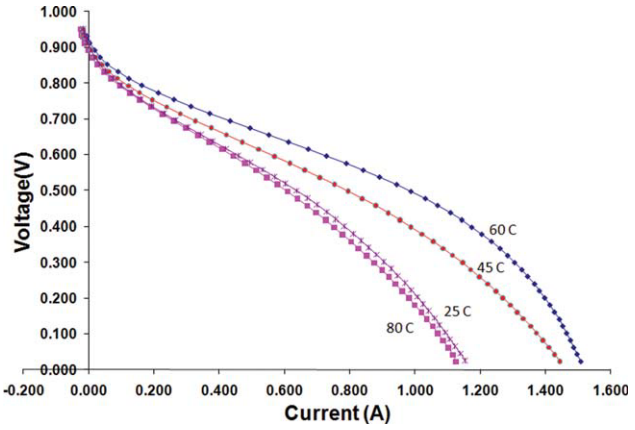

Figure 6. IV curves for the STR PEM fuel cell at a total pressure of 1 bar at temperatures of 25–80°C.

The anode feed was 8 sccm H_2, and the cathode feed was 8 sccm O_2. [Color figure can be viewed in the online issue, which is available at wileyonlinelibrary.com.]

mass transport limited current and ohmic limited current occurred circa oxygen mole fraction 0.1–0.2, suggesting that the change between pure oxygen and air feed at the cathode may introduce a change in the rate limiting step in a PEM fuel cell.

The IV curves at different temperatures shifted upward with temperature from 25 to 60°C, but then decreased as the temperature was increased to 80°C. Results for 100% oxygen feed at the cathode are shown in Figure 6; similar results were obtained at all O_2/N_2 feed ratios. At every temperature tested the relative humidity sensors at the outlets showed that the gases were ~100% RH and current interrupt measurements showed the membrane resistance decreased with increasing temperature (shown in Figure 7). The decreased resistance with increasing temperature should shift the IV curve upward. Gas phase diffusivities also increase with temperature that should also shift the IV curves upward. Countering the effect of decreased membrane resistance increased diffusivity is increased transport resistance across the GDL caused by dilution of hydrogen and oxygen concentrations with water vapor at higher temperature.

Comparison of oxygen and air feeds to a parallel flow channel PEM fuel cell

Figure 8 shows the total current from fuel cells with different MEA widths operated with constant load resistance with either pure O_2 or air feeds. The catalyst under the channel was fixed while the amount of catalyst available under the land was varied. The current increased linearly as a function of MEA width when the fuel cell cathode was fed with pure O_2 at a flow rate >2 μm/s (corresponding to a current density of 80 mA/cm^2). Decreasing the O_2 flow to 1 μm/s starved the fuel cell for reactant at MEA widths >8 mm; the current plateaued at a value equivalent to the molar O_2 feed. When air was fed to the fuel cell, the currents were reduced compared to feeding oxygen at the same molar flow rate of oxygen. Even when there is stoichiometric excess O_2 in the air feed, the current did not increase with MEAs wider than 8 mm.

The fuel cell current with O_2 feed to the cathode is well approximated by Eq. 5. There is constant current density as long as the molar O_2 feed ($F_{O_2}^{\text{cathode}}$ exceeds the ohmic-limited current, i_{ohmic}. When the oxygen feed is reduced to less than the ohmic-limited current it limits the total current.

$$i = \begin{cases} i_{\text{ohmic}} = \frac{V_{\text{effective}}}{\frac{l_{\text{mem}}}{A_{\text{MEA}}} + R_{\text{L}}} & F_{O_2}^{\text{cathode}} > i_{\text{ohmic}}/4\boldsymbol{F} \\ 4\boldsymbol{F}\, F_{O_2}^{\text{cathode}} & F_{O_2}^{\text{cathode}} < i_{\text{ohmic}}/4\boldsymbol{F} \end{cases} \tag{5}$$

The effective voltage is approximately the open circuit voltage less the activation potential, $V_{\text{effective}} \approx V_{\text{OC}} - \eta_{\text{act}} = 0.85$ V (this can be found by extrapolating the linear ohmic polarization region back to zero current).

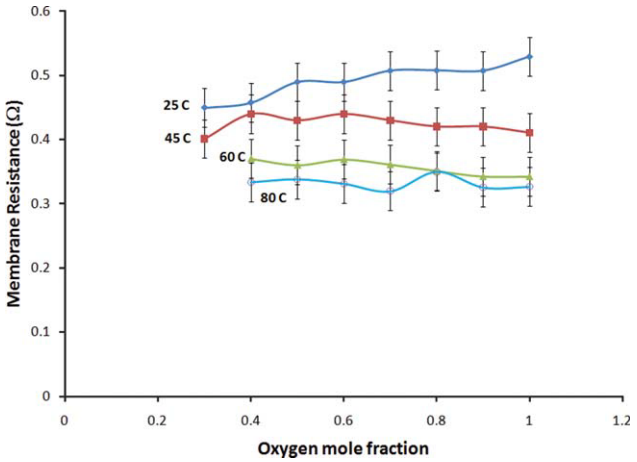

Figure 7. Internal resistance measurements of the STR PEM fuel cell operating at different temperatures with different levels of oxygen in the cathode feed.

The values are the average of the membrane resistance immediately before and after the IV sweep experiments shown in Figure 3. [Color figure can be viewed in the online issue, which is available at wileyonlinelibrary.com.]

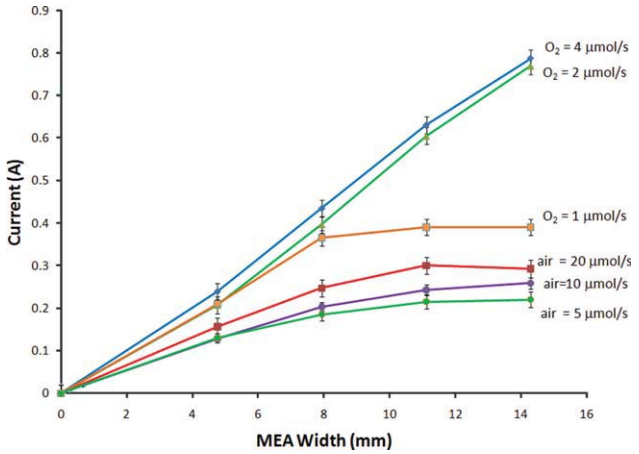

Figure 8. Current as a function of the width of the MEA in a parallel flow channel PEM fuel cell.

The experiments were all done with the same load impedance of 0.5 Ω. The gas flow channels are 1.6 mm wide. [Color figure can be viewed in the online issue, which is available at wileyonlinelibrary.com.]

The data with an air fed fuel cell show lower currents than predicted by Eq. 5, even when there is excess O_2 available. The decreased current, when replacing O_2 with air, may be accounted for by O_2 mass transport limitations across the cathode GDL.

According to Eq. 5 the current should decrease with increasing load resistance. The effect of load resistance on the oxygen mass transport limitations is demonstrated in Figure 9, where the current was measured as a function of R_L for different MEA widths. Greater load resistance results in reduced current density and the difference in the current density between an oxygen fed and an air fed fuel cell is less.

Discussion

At high current density in a PEM fuel cell, mass transport can limit the current.[1,22] Many models have been developed for gas phase transport in the GDL,[23–38] but only a few experimental studies have attempted to quantify the effects of cathode gas composition on fuel cell performance.[12,39–41] Those studies have observed that changing from O_2 to air or O_2/He mixtures causes downward shifts in the IV curves. The previous studies employed serpentine or sets of straight gas flow channels, where compositional effects along the length of the flow channel make it difficult to quantify the results. The results presented here employ simplified flow fields where the local gas compositions in the gas flow channels are well defined. The key results presented here are:

(1) Dilution of oxygen by nitrogen reduces the voltage at fixed current by a factor of 10 more than predicted by the Nernst equation.

(2) At low oxygen mole fraction in the cathode gas flow channel the current density is limited by oxygen mass transport across the GDL. As the oxygen mole fraction is increased, the limiting resistance changes and the current density becomes ohmically limited by the load resistance.

(3) Above 60°C water vapor dilutes the oxygen mole fraction and increases oxygen mass transport resistance across the cathode GDL.

(4) Oxygen mass transport from the gas flow channel to the catalyst layer under the land limits catalyst utilization when the cathode is fed by air.

Good performance of PEM fuel cells with air feeds requires that the area under the land be designed to permit oxygen to reach the entire catalyst layer. A number of investigators have considered how physical factors of the structure of the GDL and catalyst layers affect transport. Factors such as particle sizes, catalyst loading, Teflon and Nafion loading all affect the rates of transport through the GDL and have been considered by other authors.[30,42–49] Our focus is to illuminate differences in PEM fuel cell operation between air and O_2.We present models of gas transport processes in the GDL of a PEM fuel cell elucidate differences in operation and design for PEM fuel cells operated with air as opposed to oxygen.

The transition between ohmic and mass transport limited current

Figure 5 showed a transition in limiting resistance as a function of oxygen mole fraction in the cathode gas flow channel. When $x_{O_2} > 0.2$, the current was almost constant with increasing oxygen mole fraction; but at $x_{O_2} < 0.1$, the current increased linearly with oxygen mole fraction. These two regimes represent (a) the ohmic limited current at high oxygen mole fraction (the current is limited by the ohmic resistance of the load) and (b) the mass transport limited current at low oxygen mole fraction (the current is limited by oxygen mass transport from the cathode gas flow channel to the cathode catalyst layer). Figure 10 highlights the two transport resistances—diffusion of oxygen across the GDL and the ohmic current across the membrane. For simplicity the catalyst layer is assumed to be zero thickness where the

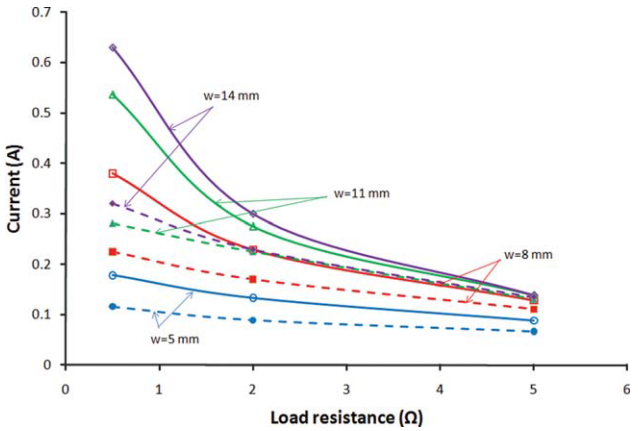

Figure 9. Comparison of current as a function of load resistance at different MEA widths with air and with oxygen as the cathode feed.

All were done with a minimum of 50% excess stoichiometry for oxygen. All experiments were done with feeds of 6 μm H_2/s at the anode and 3 μm O_2/s or 15 μm air/s at the cathode (a minimum of 50% stoichiometric excess O_2 in all cases). Solid lines are O_2 feed, dashed lines are air feed. Lines of the same color correspond to equal O_2 molar flows. [Color figure can be viewed in the online issue, which is available at wileyonlinelibrary.com.]

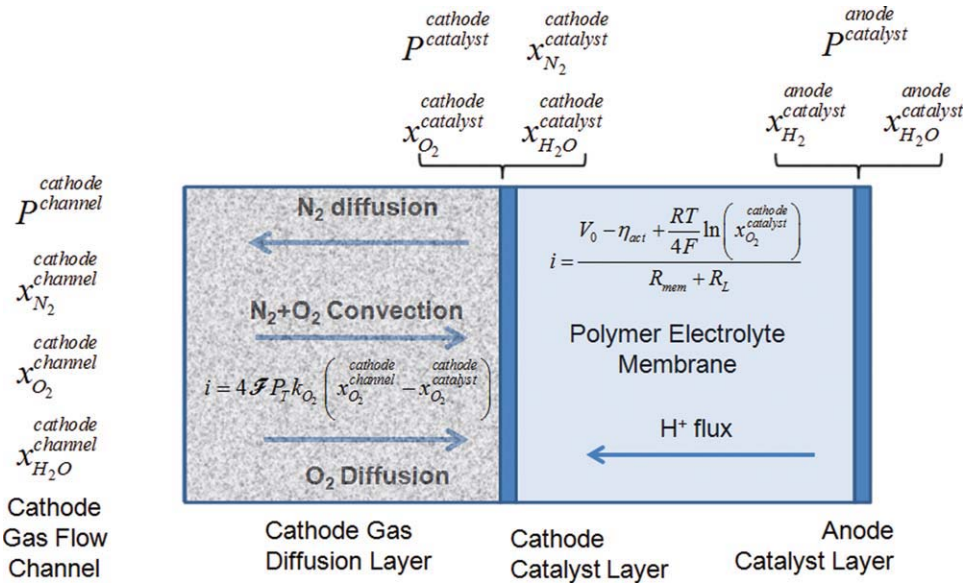

Figure 10. Schematic of a PEM fuel cell with transport resistances across the cathode GDL and the polymer electrolyte membrane.

Oxygen is consumed by reaction at the catalyst layer, driving both convective and diffusive flows across the GDL. Convection is driven by a pressure difference resulting from a reduction in molar concentration associated with oxygen consumption at the catalyst. Diffusion across the cathode GDL is driven by the concentration difference between the gas flow channel and the catalyst layer. The proton current is driven by the chemical potential difference between the chemical potential of hydrogen at the anode and cathode catalyst layers. [Color figure can be viewed in the online issue, which is available at wileyonlinelibrary.com.]

electrochemical reactions are fast, and the potential of the fuel cell can be approximated as the thermodynamic voltage less the activation potential.

At steady state, the current density across the MEA is equal to the molar flux of oxygen across the GDL and to the proton current across the PEM (divided by 4 times Faraday's constant) as shown by Eq. 6. The effective oxygen mass transport coefficient, k_{O_2}, is equal to the slope of current vs. oxygen mole fraction graph (Figure 5) in the mass transport limited regime (at $x_{O_2} \to 0$); $4\boldsymbol{F}\ k_{O_2} = 6.3$ A/cm^2 bar for the Etek GDL employed in this study. The proton current density is given by the effective voltage difference between the anode and cathode catalyst layers divided by the sum of the areal resistivity of the membrane and the load resistance. The effective voltage is the thermodynamic potential less the activation overpotential. At open circuit the compositions at the catalyst layers are the same as in the gas flow channels; however, when the fuel cell delivers a current, the oxygen concentration at the cathode catalyst layer is less than that in the cathode flow channel (an analogous situation exists for hydrogen at the anode catalyst layer). The third term in the numerator in Eq. 6 represents the reduction of the thermodynamic voltage because of the reduced oxygen concentration at the catalyst layers.

$$j = 4\boldsymbol{F}k_{O_2,GDL}P_T\left(x^{cathode}_{O_2,channel} - x^{cathode}_{O_2,catalyst}\right) = \frac{V_{oc} - \eta_{act} + \frac{RT}{2\boldsymbol{F}}\ln\left(\frac{x^{anode}_{H_2,catalyst}\left(x^{cathode}_{O_2,catalyst}\right)^{1/2}}{x^{cathode}_{H_2O,catalyst}}\right)}{\rho_{membrane} + R_L A_{MEA}} \quad (6)$$

When the fuel cell is operated at 100% RH the mole fraction of water is equal to the saturation pressure of water divided by the total pressure, $x_{H_2O} = P^0_{H_2O}/P_T$ at both the cathode and anode flow channels, the catalyst layers and across the GDLs. For a pure hydrogen feed the mole fraction of hydrogen is essentially the same in the anode gas flow channel and at the anode catalyst layer, $x^{anode}_{H_2,channel} = x^{anode}_{H_2,catalyst} = 1 - x_{H_2O}$. Equations 4 and 6 can be solved for oxygen mole fraction at the cathode catalyst layer and the current density as a function of oxygen mole fraction in the cathode feed and the molar feed rate to the cathode. The mass transport limited current is given by Eq. 6 when $x^{cathode}_{O_2,catalyst} \to 0$. Equation 6 was solved using $R_{membrane} = 0.46\ \Omega$, determined from current interrupt measurements, and $4\boldsymbol{F}\ k_{O_2,GDL} = 6.3$ A/cm^2 bar. The solid lines in Figure 5 are the calculated values from Eq. 6 assuming excess hydrogen at the anode ($x^{anode}_{H_2} = 1 - (P^0_{H_2O}/P_T)$) and water saturated conditions at the cathode.

Oxygen convection and diffusion across the GDL

Equation 6 described O_2 transport across the GDL with a lumped mass transport coefficient. Oxygen is transported across the cathode GDL by a combination of pressure driven convection through the porous GDL and concentration driven diffusion, as summarized in Figure 10. Consider the situation of 100% RH in the cathode gas flow channel, which is consistent with our experimental results and is also the situation encountered in most PEM fuel cells. Because the vapor in the cathode gas flow channel is saturated with water vapor, additional water produced at the cathode must be immediately condensed. When oxygen is consumed at the cathode catalyst

layer, there is a reduction of the total pressure due to the reduction in the total number of moles in the vapor. The differential pressure between the cathode flow channel and cathode catalyst layer drives a convective flow of air with nitrogen, oxygen and water vapor through the porous media. At the catalyst layer oxygen is consumed and nitrogen accumulates. What is the relative importance of convection to diffusion through the GDL? Most models of lateral mass transport through the GDL with serpentine flow systems have focused on diffusive transport in the GDL based on the Stefan Maxwell equations.[1] A number of recent models in the literature have included convective flow in the porous GDL via Darcy's law.[23–38,49] Studies with interdigitated flow fields have shown that pressure driven flows through the cathode GDL give rise to higher current densities than serpentine of parallel channel systems. Models with both serpentine and straight flow channels that have included convective flow in the GDL find small pressure differences across the GDL, suggesting that convection is negligible, and it is adequate to assume uniform pressure across the GDL.

It is impossible to have an oxygen concentration gradient to drive diffusion from the cathode flow channel to the cathode catalyst layer without a nitrogen concentration gradient that carries nitrogen from the cathode catalyst layer back to the cathode flow channel. The only way to have a higher nitrogen concentration at the cathode catalyst layer is for nitrogen to be convected to the catalyst layer. The convective molar flow of nitrogen, F_{N_2} across the cathode gas flow channel to the catalyst layer can be described by Darcy's law through a porous medium with permeability κ and uniform pores of radius r_p. The molar flux of nitrogen is then given by Eq. 7, where μ is the gas viscosity, P is the local pressure and z is the distance from the gas channel/GDL interface.

$$\left(\frac{F_{N_2}}{A_{MEA}}\right)_{convection} = -x_{N_2}\frac{\kappa}{\mu}\frac{P}{RT}\left(-\frac{dP}{dz}\right) \tag{7}$$

For a uniform porous medium the permeability is given by Eq. 8 where ε is the void fraction and τ is the tortuosity of the porous medium.

$$\kappa = \frac{r_p^2}{8}\frac{\varepsilon}{\tau} \tag{8}$$

The diffusive nitrogen flux from the catalyst layer to the gas flow channel is given by Fick's law in Eq. 9.

$$\left(\frac{F_{N_2}}{A_{MEA}}\right)_{diffusion} = -\frac{P}{RT}D_{N_2}\frac{\varepsilon}{\tau}\left(\frac{dx_{N_2}}{dz}\right) \tag{9}$$

The diffusion coefficient has been corrected by the void fraction and tortuosity of the porous medium. At steady state the (convective) flux of nitrogen to the catalyst layer is equal to its (diffusive) flux back to the gas flow channel; equating (7) and (9) gives the relation between the pressure gradient to the concentration gradient.

$$\frac{dP/dz}{dx_{N_2}/dz} = \frac{D_{N_2}\mu}{\left(r_p^2/8\right)} \tag{10}$$

Substituting in values for the properties of air and the GDL into Eq. 10 ($D_{N_2} = 0.2$ cm$^2/s$, $\mu = 2 \times 10^{-4}$ g/cm $- s$ $r_p = 10^{-3}$ cm) provides an order of magnitude estimate of the pressure difference across the GDL as a function of the nitrogen mole fraction difference, $(dP/dx_{N_2}) = 0.032$ bar. The maximum pressure difference across the GDL would correspond to pure nitrogen at the catalyst layer $\Delta x_{N_2} = 1$, giving a maximum pressure drop of 0.03 bar. Typical operating pressures of PEM fuel cells are 1–3 bar so that for diffusion calculations it is reasonable to assume the pressure across the GDL is nearly constant.

However, even though the pressure drop across the GDL is small, the convective flux of oxygen is non-negligible in comparison to its diffusive flux. The total oxygen flux is equal to the sum of the convective flux of oxygen that is carried along with the nitrogen driven by the pressure difference plus the diffusive flux driven by the oxygen concentration difference, as shown in Eq. 11.

$$\begin{aligned}\text{oxygen flux} &= \frac{x_{O_2}}{x_{N_2}}(\text{nitrogen flux}) + \frac{P_T}{RT}D_{O_2}\frac{\varepsilon}{\tau}\frac{dx_{O_2}}{dz} \\ &= \frac{x_{O_2}}{x_{N_2}}\left(\frac{P_T}{RT}D_{N_2}\frac{\varepsilon}{\tau}\left(-\frac{dx_{N_2}}{dz}\right)\right) + \frac{P_T}{RT}D_{O_2}\frac{\varepsilon}{\tau}\frac{dx_{O_2}}{dz} \\ &= \frac{P_T}{RT}\frac{\varepsilon}{\tau}\left(\frac{x_{O_2}}{x_{N_2}}D_{N_2} + D_{O_2}\right)\frac{dx_{O_2}}{dz}\end{aligned} \tag{11}$$

When the nitrogen concentration in the cathode gas flow channel is small, the gradient in the nitrogen concentration becomes large and the flux of oxygen is primarily by convection (the first term on the right hand side at the top of Eq. 11). The last line in Eq. 11 appears to suggest that oxygen is only transported by diffusion. That is because the convective flux of nitrogen to the catalyst layer is equal to its reverse diffusive flux. It takes a very small pressure differential to drive a convective flow that exceeds the diffusive transport. For pure oxygen, $x_{N_2} = 0$ Eq. 11 indicates the oxygen flux becomes infinite and there is no concentration gradient across the GDL. This is of course impossible and is the result of equating the nitrogen and oxygen concentration gradients which is becomes meaningless in the absence of nitrogen. At zero nitrogen concentration the oxygen transport across the GDL is entirely convection driven. When the nitrogen concentration is high the convective flow becomes small relative to the diffusive flow.

The flux of oxygen across the GDL is balanced by the oxygen consumption at the catalyst layer, which is equal to the current density.

$$\text{oxygen convection} + \text{oxygen diffusion} = \text{oxygen consumption}$$

$$\frac{P_T}{RT}\frac{\varepsilon}{\tau}\left(\frac{x_{O_2}}{x_{N_2}}D_{N_2} + D_{O_2}\right)\frac{dx_{O_2}}{dz} = \frac{j}{4F} \tag{12}$$

Equation 12 can be simplified through a few approximations to Eq. 13. The diffusivities of oxygen and nitrogen are nearly the same and can be assumed equal. Assuming the gas is water saturated everywhere, the mole fraction of nitrogen can be expressed in terms of the saturation vapor pressure of water and the mole fraction of oxygen.

$$\underbrace{\frac{1 - x_{H_2O}}{(1 - x_{O_2} - x_{H_2O})}}_{\text{correction term}}\ \underbrace{D_{O_2}\frac{\varepsilon}{\tau}\frac{P^{channel}}{RT}\frac{dx_{O_2}}{dz}}_{\text{diffusive term}} = \frac{j}{4F} \tag{13}$$

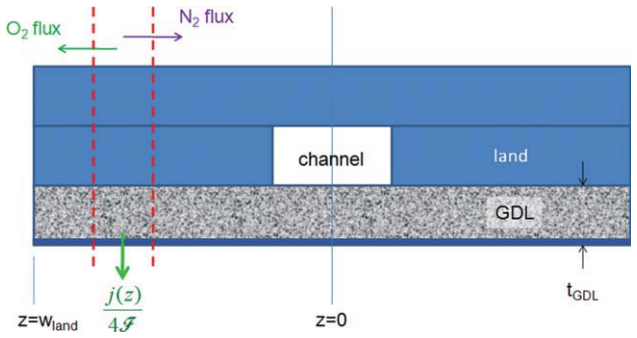

Figure 11. Schematic of oxygen transport from the gas flow channel to the catalyst layer.

[Color figure can be viewed in the online issue, which is available at wileyonlinelibrary.com.]

Equation 13 looks like the normal diffusion equation with a correction term that accounts for the relative importance of convection to diffusion. As the oxygen mole fraction goes to zero, oxygen is only transported by diffusion; at large oxygen mole fraction the transport is greatly enhanced by convection. Equation 13 is significant in showing that the predominant mode of oxygen transport changes from convective flow to diffusive flow as the oxygen mole fraction is reduced. In a 2D flow field with an air fed fuel cell, oxygen will be depleted along the length of the flow channel the balance between convective and diffusive transport will change which will affect catalyst utilization.

We have not included any analysis about the hydrogen mass transport across the GDL at the anode. However, if one follows a similar analysis for the anode with a pure hydrogen feed, hydrogen transport across the anode GDL will be mainly by convection, and the hydrogen mole fraction at the anode catalyst layer will be nearly equal to the hydrogen mole fraction in the anode gas flow channel.

Oxygen mass transport under the land

The switch from pure oxygen to air has a large effect on the utilization of the catalyst under the land in a parallel flow channel PEM fuel cell. The entire width of the catalyst under the land was active when pure oxygen was fed to the PFC fuel cell, but only a limited part of the catalyst layer was active when air was fed instead. As shown schematically in Figure 11, oxygen must be transported through the GDL in both the transverse and lateral directions to the catalyst layer. Because the distance for diffusion under the land is generally greater than the thickness of the GDL, we anticipate significant diffusional limitations for oxygen to reach the cathode catalyst layer further under the land when the oxygen is diluted by nitrogen.

Oxygen travels both laterally and transversely from the flow channel to the catalyst layer. The lateral flux changes as a function of distance because oxygen is consumed by reaction under the land. The local current density at the catalyst layer is a function of the local concentrations. This is a two dimensional transport equation where flux boundary conditions are known at the GDL interfaces (GDL/channel, GDL/land and GDL/catalyst interfaces). Because the width of the GDL under the land, w_{land}, is generally much greater than the thickness of the GDL t_{GDL}, ($w_{land}/t_{GDL} \sim 10$) the diffusion may be approximated as one dimensional laterally through the GDL under the land.

The lateral flux of oxygen through the GDL changes due to consumption of oxygen at the cathode catalyst layer as expressed in Eq. 14. Variations in the transverse direction have been ignored here; these must, of course, be included for quantitative modeling.

$$L_{channel} t_{GDL} \Delta(\text{Flux}) = L_{channel} t_{GDL} \Delta \times \left[\frac{x_O}{x_N} \frac{P}{RT} D_{e,N} \left(-\frac{dx_N}{dz} \right) + D_{e,O} \frac{P}{RT} \left(\frac{dx_O}{dz} \right) \right] = L_{channel} \Delta z \frac{j(z)}{4F} \tag{14}$$

The two terms in parentheses in (14) represent the convective flux associated with the nitrogen flow and the diffusive flux associated with the oxygen concentration gradient; D_e are effective diffusivities that account for porosity and tortuosity, P is the total (and for our purposes here, effectively constant) pressure in the GDL and the mole fractions are averaged values across the GDL (in the y direction) at position z. The right hand side of Eq. 14 is the oxygen consumption by reaction at the catalyst layer; the current will depend on the local oxygen mole fraction at position z. Equation 15 assumes that the species concentrations across the GDL in the y direction are uniform, which is not correct. To get the local current density as a function of the local oxygen mole fraction we will employ Eq. 6, substituting $x_O(z)$ for $x_{O_2}^{channel}$ and $k_{O_2} = D_e/RT t_{GDL}$. Equation 14 can be simplified by assuming the diffusivities of oxygen and nitrogen are the same, the mole fraction of water vapor is constant everywhere and the pressure is constant.

$$t_{GDL} \frac{P}{RT} D_e \frac{d}{dz} \left[\frac{x_{O_2}}{x_{N_2}} \left(\frac{dx_{O_2}}{dz} \right) + \left(\frac{dx_{O_2}}{dz} \right) \right] = \frac{j(z)}{4F}$$

$$t_{GDL} \frac{P}{RT} D_e \frac{d}{dz} \left[\frac{1 - x_{H_2O}^{channel}}{\left(1 - x_{O_2} - x_{H_2O}^{channel}\right)} \left(\frac{dx_{O_2}}{dz} \right) \right] = \frac{j(z)}{4F} \tag{15}$$

B.C.

$$x_{O_2} = x_{O_2}^{channel} \quad \text{at} \quad z = 0$$

$$\frac{dx_{O_2}}{dz} = 0 \quad \text{at} \quad z = w_{land}$$

Equation 15 was integrated to evaluate the current as a function of the width of the GDL under the land for humidified oxygen and humidified air in the cathode flow channel at different load impedances. Figure 12 presents a comparison of the integrated current for oxygen vs. air feed to a 6.1 cm long PFC fuel cell with different widths under the land at two different load impedances, analogous to the experimental results shown in Figure 8 and 9. The simplified one-dimensional model does a remarkable job matching the data obtained at 0.5 Ω (see Figure 8). All the parameters were determined from independent experiments. The model predicts that the current increases linearly with GDL width when the cathode feed is pure oxygen, while it plateaus with an air feed. The results also show that there is less effect with higher load resistance; the currents are reduced and the current becomes ohmic limited, not limited by mass transport.

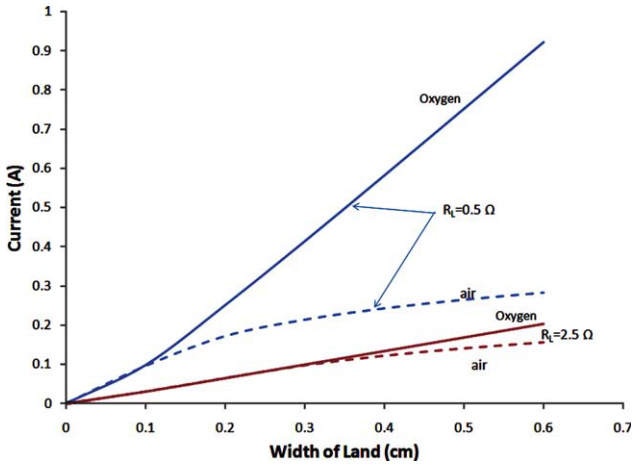

Figure 12. Total current as a function of width of the GDL under the land in a single channel PEM fuel cell based on the model Eqs. 6 and 15.

[Color figure can be viewed in the online issue, which is available at wileyonlinelibrary.com.]

Figure 13 compares the ratio of the current with air feed to the current with pure oxygen feed at different load resistances as a function of the width of the GDL under the land. As the load resistance increases, reducing the current, the effect of switching between oxygen and air is reduced. It is also clear that at high load resistances, the width of the GDL under the land can be increased without having significant mass transport resistances; of course high load resistances result in low current densities and reduced power output for the fuel cell. Sun et al. presented a model that showed that with an air fed cathode mass transport limitations were most important at large overpotential,[13] corresponding to high load resistance.

Implications for fuel cell design and modeling

In designing flow fields for PEM fuel cells, catalyst utilization is essential because of the high cost of Pt catalysts. To effectively utilize the catalyst, the current should not be limited by oxygen mass transport. Hence the lateral flux through the GDL should be sufficient to provide reasonably uniform current density to the area under the land. Equation 16 is an integrated form of Eq. 15 where dx_{O_2}/dz has been approximated by the mole fraction difference between the cathode gas flow channel and the catalyst layer at a distance w_{land} away from the gas flow channel divided by the width of the land.

$$\begin{matrix}\text{lateral flux across GDL} & > & \text{current}\end{matrix}$$

$$t_{GDL}4F\left[\frac{1-x_{H_2O}^{channel}}{1-x_{H_2O}^{channel}-x_{O}^{channel}}\frac{D_eP}{RT}\frac{\left(x_{O_2}^{channel}-x_{O_2}^{GDL,w_{land}}\right)}{w_{land}}\right] > \frac{V_{oc}-\eta_{act}}{R_L+\rho_{membrane}/Lw_{land}} \quad (16)$$

Assuming $x_{O_2}^{GDL,w_{land}}=0$ and $R_L \gg \rho_{membrane}/Lw_{land}$ Eq. 16 can be simplified to give a limit on the ratio of the width of the land to the thickness of the GDL for good catalyst utilization; the parameters are the composition in the gas flow channel and the load resistance.

$$\frac{w_{land}}{t_{GDL}} < \left[\frac{\left(1-x_{H_2O}^{channel}\right)x_{O_2}^{channel}}{1-x_{H_2O}^{channel}-x_{O_2}^{channel}}\frac{D_eP}{RT}\frac{V_{co}-\eta_{act}}{4FR_L}\right] \quad (17)$$

Equation 17 reveals that the greater the oxygen mole fraction in the cathode gas flow channel the wider the useful area of the GDL under the land. Furthermore, Eq. 17 shows that making the GDL layer thinner requires reduced width of the GDL under the land for good catalyst utilization, because the gas flow is more restricted.

Several models presented in the literature have been solved numerically, showing the same trends in diffusional limitations indicated by Eq. 17[11–13,15,50] The models have suggested similar conclusions to those presented here: larger effective diffusivity in the GDL and larger channel to land ratios are important for good catalyst utilization. We have isolated the roles of convection and diffusion as a function of gas composition at the cathode with the experiments and our simplified model. Equation 17 can be thought of as a useful approximate reduction of the dimensionality from 2 to 1 spatial dimensions. Weber recently published an analytic solution for an effective GDL thickness to channel length for the channel and land that is analogous to Eq. 17.[51] His goal was also to achieve reduction in the dimensional order of PEM fuel cell models.

Most fuel cell manufacturers prefer operation with air as the source of oxygen at the cathode, since it doesn't require a second gas storage tank. Many experimental studies have compared fuel cell operation with oxygen and air through the IV curves, and it is always observed that the voltage is reduced with air feed compared to oxygen feed in both the ohmic polarization regime and the mass transport limited regime. Rho et al. obtained polarization data at different oxygen mole fractions in the feed (similar to the results presented here).[39,40] In fitting their data, they suggested that the membrane resistance was a function of oxygen mole fraction and pressure. The membrane resistivity is only dependent on

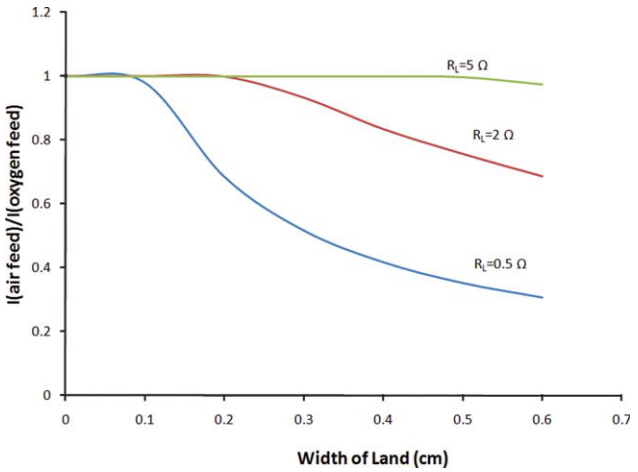

Figure 13. Ratio of the current with air feed to the current with oxygen feed for the same load impedance and same width of GDL under the land.

[Color figure can be viewed in the online issue, which is available at wileyonlinelibrary.com.]

water activity. As we have shown here, the reduction of the voltage results from both lateral and transverse oxygen mass transport resistance across the cathode GDL.

The most significant result reported here is the role of mass transport laterally from the gas flow channel through the GDL to the catalyst layer beneath the land. This has a large impact on the effective utilization of catalyst at the cathode of the GDL when air is used as the feed to the cathode. Even with large stoichiometric excesses of air, there were substantial reductions of the current when the land/channel ratio exceeded 2.

Natarajan and Van Nguyen previously reported a transition to a mass transported limited current due to oxygen depletion along the length of a single channel fuel cell with a segmented electrode.[12,52] Van Nguyen and coworkers have also shown the diffusional limitations at the cathode can be reduced by forcing the flow through the GDL with interdigitated flow fields.[33,38,53] Our results build upon previously semiquantitative observations and provide direct measurements of the diffusional limits with well defined composition measurements.

The results in Figure 5 show that mass transport limitations become significant when the oxygen mole fraction in the cathode gas flow channel falls below 0.2, which just happens to correspond to the composition of air. There are several approaches that can be applied to the problem of mass transport limitations at the cathode. The simplest is to employ thin GDLs with wide gas flow channels and narrow lands. This solution could create problems with water removal, because the gas velocities would be reduced in the wide channels and the gas would be less effective at pushing out liquid water drops.[54] An alternative solution would be to incorporate an air separation membrane as part of the cathode feed to supply oxygen enriched air to the cathode. It is important to note that high purity oxygen is not essential to reduce the mass transport limitations—it is sufficient to have an enriched feed with 40–60% oxygen to greatly reduce the mass transport limitations! A third approach is to force convective flow through the GDL under the land using interdigitated dead ended flow channels.[33,55–57] This design as originally developed was conceived to push liquid water that had condensed in the GDL. Recent studies show that the water content in the GDL is small, and there is probably no need to push the gas flow through the GDL to overcome liquid flooding; but the interdigitated flow fields can be very effective in alleviating oxygen mass transport resistances through the GDL under the land.

The analysis presented in this article has emphasized the mass transport limitations at the cathode. It was pointed out that, with pure oxygen, the mass transport limitations are greatly reduced, because the convective transport is dominant and there is little difference in composition between the flow channel and at the catalyst layer. Because the anode generally employs high purity hydrogen feeds, the supply of hydrogen to the anode catalyst layer will be primarily convection driven by a small pressure differential between the anode flow channel and the anode catalyst layer. If one were to employ H_2/CO_2 mixtures from steam reformate as the anode feed, the issues of mass transport resistance would become important at the anode as well. The problem of hydrogen mass transport from reformate streams has been examined in more detail for hydrogen purification using a Polymer Electrolyte Hydrogen Pump reported elsewhere.[58]

Conclusions

The effect of oxygen dilution at the cathode on PEM fuel cell performance was examined. Employing air as the source of oxygen at the cathode of PEM fuel cells significantly reduces the current (or voltage) of a PEM fuel cell. Lateral oxygen transport from the cathode gas flow channel to the cathode catalyst layer under the land greatly reduces the local current density and fuel cell efficacy.

The key results from this study are:

(1) Oxygen dilution by nitrogen increases mass transport resistance from the gas flow channel to the cathode catalyst layer.

(2) At high oxygen mole fraction in the cathode gas channel, the current is limited by the ohmic resistance of the load resistance. At low oxygen mole fraction in the cathode gas flow channel, the current is limited by oxygen mass transport across the cathode GDL.

(3) Oxygen transport across the GDL is driven by both convection and diffusion. Convection is dominant at high oxygen mole fraction and diffusion is dominant at low oxygen mole fraction.

(4) Oxygen transport from the cathode gas flow channel to the cathode catalyst layer under the lands is limited with air feeds, reducing the total current. There is a critical width of the land beyond which the cathode catalyst layer is not utilized.

(5) Proper physical descriptions of transport processes in the GDL appear to be more important to predictive models for PEM fuel cells than complex electrochemical kinetics.

Acknowledgments

The authors thank the NSF (CTS 0754715) for support of this work. E. Kimball thank the Princeton University Program in Plasma Science and Technology for partial support under U.S. Department of Energy, Contract No. DE-AC02-76-CHO-3073. R. Meija-Ariza thank the NSF for REU support through the Princeton Institute for the Science and Engineering of Materials.

Notation

A_{mem} = area of membrane (cm^2)
D_{N_2} = diffusivity of nitrogen (cm^2/s)
D_{O_2} = diffusivity of oxygen (cm^2/s)
D_{e,N_2} = effective diffusivity of nitrogen in the GDL (cm^2/s)
D_{e,O_2} = effective diffusivity of oxygen in the GDL (cm^2/s)
$F_{H_2}^{feed}$ = molar flow of hydrogen in the anode feed (mol/s)
$F_{H_2}^{anode}$ = molar flow of hydrogen leaving anode (mol/s)
$F_{O_2}^{feed}$ = molar flow of oxygen in the cathode feed (mol/s)
$F_{O_2}^{cathode}$ = molar flow of oxygen leaving cathode (mol/s)
$F_{N_2}^{feed}$ = molar flow of nitrogen in the cathode feed (mol/s)
$F_{O_2}^{cathode}$ = molar flow of nitrogen leaving cathode (mol/s)
F_{N_2} = molar flux of nitrogen across the GDL (mol/cm^2 s)
$F_{H_2O}^{anode}$ = molar flow of water leaving anode (mol/s)

$F_{H_2O}^{cathode}$ = molar flow of water leaving the cathode (mol/s)
F = Faraday's constant (96,485 coulomb/mol)
GDL = gas diffusion layer
i = current (amp)
i_{ohmic} = current limited by load resistance (amp)
I = current across load resistance (amp)
j = current density (amp/cm^2)
j_{max} = maximum current density for a given load resistance
$k_{O_2,GDL}$ = effective mass transport coefficient for oxygen transport across the GDL (mol/bar)
$L_{channel}$ = length of flow channel in PFC fuel cell (cm)
$P_{H_2O}^0$ = vapor pressure of water
P_T = total pressure in the fuel cell
PEM = polymer electrolyte membrane
PFC = parallel flow channel
$R_{membrane}$ = load resistance (ohm)
R_L = load resistance (ohm)
R_H = hydraulic radius of gas flow channel
r_p = pore radius of GDL pores (cm)
STR = stirred tank reactor
T = temperature (K)
t_{GDL} = thickness of GDL (cm)
V = voltage drop across load resistance (volt)
$V_{effective} = (V_{oc} - \eta_{act})$ = effective voltage in the ohmic regime of fuel cell ($\sim$0.85 V)
V_{oc} = open circuit voltage ($\sim$1.2 V)
w_{land} = width of the MEA under the land (cm)
$x_{H_2}^{feed}$ = molar fraction of hydrogen in the feed
$x_{H_2}^{anode}$ = molar flow of hydrogen leaving anode
$x_{H_2}^{anode\ catalyst}$ = mole fraction of hydrogen in anode catalyst layer
$x_{H_2}^{anode\ channel}$ = mole fraction of hydrogen in the anode gas flow channel
$x_{O_2}^{feed}$ = mole fraction oxygen in the cathode feed
$x_{O_2}^{cathode}$ = mole fraction oxygen leaving the cathode
$x_{O_2}^{cathode\ catalyst}$ = mole fraction oxygen at the cathode
$x_{O_2}^{cathode\ channel}$ = mole fraction oxygen in the cathode flow channel
$x_{N_2}^{feed}$ = mole fraction nitrogen in the cathode feed
$x_{N_2}^{cathode}$ = mole fraction nitrogen leaving the cathode
$x_{N_2}^{cathode\ catalyst}$ = mole fraction nitrogen in the cathode catalyst layer
$x_{N_2}^{cathode\ channel}$ = mole fraction nitrogen in the cathode gas flow channel
$x_{H_2O}^{cathode\ channel}$ = mole fraction water vapor in the cathode gas flow channel
$x_{H_2O}^{anode\ channel}$ = mole fraction watervapor in the anode gas flow channel
ε = void fraction in the GDL
κ = Darcy's law permeability (cm^2)
μ = gas viscosity in the GDL (g cm^2/s)
ρ_{mem} = arial resistivity of membrane (ohm cm^2)
τ = tortuosity of the GDL

Literature Cited

1. Weber AZ, Newman J. Modeling transport in polymer-electrolyte fuel cells. *Chem Rev*. 2004;104:4679–4726.
2. Thampan T, Malhotra S, Zhang JX, Datta R. PEM fuel cell as a membrane reactor. *Catal Today*. 2001;67:15–32.
3. Pasaogullari U, Wang CY. Liquid water transport in gas dissusion layer of polymer electrolyte fuel cells. *J Electrochem Soc*. 2004;151:A399–A406.
4. Wang CY. Fundamental models for fuel cell engineering. *Chem Rev*. 2004;104:4727–4766.
5. Wang ZH, Wang CY, Chen KS. Two-phase flow and transport in the air cathode of proton exchange membrane fuel cells. *J Power Sources*. 2001;94:40–50.
6. Benziger J, Nehlsen J, Blackwell D, Brennan T, Itescu J. Water flow in the gas diffusion layer of PEM fuel cells. *J Memb Sci*. 2005;261:98–106.
7. Kimball E, Whitaker T, Kevrekidis YG, Benziger JB. Drops, slugs, and flooding in polymer electrolyte membrane fuel cells. *AIChE J*. 2008;54:1313–1332.
8. Litster S, Sinton D, Djilali N. Ex situ visualization of liquid water transport in PEM fuel cell gas diffusion layers. *J Power Sources*. 2006;154:95–105.
9. Pasaogullari U, Wang CY. Liquid water transport in gas diffusion layer of polymer electrolyte fuel cells. *J Electrochem Soc*. 2004;151:A399–A406.
10. Hickner MA, Siegel NP, Chen KS, McBrayer DN, Hussey DS, Jacobson DL, Arif M. Real-time imaging of liquid water in an operating proton exchange membrane fuel cell. *J Electrochem Soc*. 2006;153:A902–A908.
11. Jeng KT, Lee SF, Tsai GF, Wang CH. Oxygen mass transfer in PEM fuel cell gas diffusion layers. *J Power Sources*. 2004;138:41–50.
12. Natarajan D, Van Nguyen T. Current distribution in PEM fuel cells. Part 2: air operation and temperature effect. *AICHE J*. 2005;51:2599–2608.
13. Sun W, Peppley BA, Karan K. Modeling the influence of GDL and flow-field plate parameters on the reaction distribution in the PEMFC cathode catalyst layer. *J Power Sources*. 2005;144:42–53.
14. Wang XD, Duan YY, Yan WM. Numerical study of cell performance and local transport phenomena in PEM fuel cells with various flow channel area ratios. *J Power Sources*. 2007;172:265–277.
15. Wang XD, Duan YY, Yan WM, Peng XF. Effects of flow channel geometry on cell performance for PEM fuel cells with parallel and interdigitated flow fields. *Electrochimica Acta*. 2008;53:5334–5343.
16. Wang XD, Zhang XX, Yan WM, Lee DJ, Su A. Determination of the optimal active area for proton exchange membrane fuel cells with parallel, interdigitated or serpentine designs. *Int J Hydrogen Energy*. 2009;34:3823–3832.
17. Benziger J, Chia E, Karnas E, Moxley J, Teuscher C, Kevrekidis IG. The stirred tank reactor polymer electrolyte membrane fuel cell. *AICHE J*. 2004;50:1889–1900.
18. Chia ESJ, Benziger JB, Kevrekidis LG. STR-PEM fuel cell as a reactor building block. *AICHE J*. 2006;52:3902–3910.
19. Hogarth WHJ, Benziger JB. Dynamics of autohumidifed PEM fuel cell operation. *J Electrochem Soc*. 2006;153:A2139–A2146.
20. Satterfield MB, Benziger JB. Non-Fickian water sorption dynamics by Nafion membranes. *J Phys Chem B*. 2008;112:3693–3704.
21. Majsztrik PW, Satterfield MB, Benziger J, Bocarsly AB. Water sorption, desorption and transport in Nafion membranes. *J Memb Sci*. 2007;301:93–106.
22. Srinivasan S, Dave BB, Murugesamoorthi KA, Parthasarathy A, Appleby AJ. *Overview of fuel cell technology*. In: Blomen LJMJ, Mugerwa MN, editors. *Fuel Cell Systems*. New York: Plenum Press, 1993:37–72.
23. Berg P, Novruzi A, Volkov O. Reaction kinetics at the triple-phase boundary in PEM fuel cells. *J Fuel Cell Sci Technol*. 2008;5(2):021007.
24. Berning T, Djilali N. A 3D, multiphase, multicomponent model of the cathode and anode of a PEM fuel cell. *J Electrochem Soc*. 2003;150:A1589–A1598.
25. Berning T, Lu DM, Djilali N. Three-dimensional computational analysis of transport phenomena in a PEM fuel cell. *J Power Sources*. 2002;106:284–294.
26. Bradean R, Promislow K, Wetton B. Transport phenomena in the porous cathode of a proton exchange membrane fuel cell. *Num Heat Transfer Part A: Appl*. 2002;42:121–138.
27. Bultel Y, Wiezell K, Jaouen F, Ozil P, Lindbergh G. Investigation of mass transport in gas diffusion layer at the air cathode of a PEMFC. *Electrochimica Acta*. 2005;51:474–488.
28. Dutta S, Shimpalee S, Van Zee JW. Three-dimensional numerical simulation of straight channel PEM fuel cells. *J Appl Electrochem*. 2000;30:135–146.
29. Futerko P, Hsing IM. Two-dimensional finite-element method study of the resistance of membranes in polymer electrolyte fuel cells. *Electrochimica Acta*. 2000;45:1741–1751.
30. Gostick JT, Ioannidis MA, Fowler MW, Pritzker MD. Pore network modeling of fibrous gas diffusion layers for polymer electrolyte membrane fuel cells. *J Power Sources*. 2007;173:277–290.

31. Gurau V, Liu HT, Kakac S. Two-dimensional model for proton exchange membrane fuel cells. *AICHE J*. 1998;44:2410–2422.
32. Gurau V, Zawodzinski TA, Mann JA. Two-phase transport in PEM fuel cell cathodes. *J Fuel Cell Sci Technol*. 2008;5(2):021009.
33. He WS, Yi JS, Van Nguyen T. Two-phase flow model of the cathode of PEM fuel cells using interdigitated flow fields. *AICHE J*. 2000;46:2053–2064.
34. Hsing IM, Futerko P. Two-dimensional simulation of water transport in polymer electrolyte fuel cells. *Chem Eng Sci*. 2000;55:4209–4218.
35. Jordan LR, Shukla AK, Behrsing T, Avery NR, Muddle BC, Forsyth M. Diffusion layer parameters influencing optimal fuel cell performance. *J Power Sources*. 2000;86:250–254.
36. Markicevic B, Bazylak A, Djilali N. Determination of transport parameters for multiphase flow in porous gas diffusion electrodes using a capillary network model. *J Power Sources*. 2007;171:706–717.
37. Mennola T, Noponen M, Aronniemi M, Hottinen T, Mikkola M, Himanen O, Lund P. Mass transport in the cathode of a free-breathing polymer electrolyte membrane fuel cell. *J Appl Electrochem*. 2003;33:979–987.
38. Nguyen PT, Berning T, Djilali N. Computational model of a PEM fuel cell with serpentine gas flow channels. *J Power Sources*. 2004;130:149–157.
39. Rho YW, Srinivasan S, Kho YT. Mass-transport phenomena in proton-exchange membrane fuel-cells using O_2/He, O_2/Ar and O_2/N_2 mixtures. 2. Theoretical analysis. *J Electrochem Soc*. 1994;141:2089–2096.
40. Rho YW, Velev OA, Srinivasan S, Kho YT. Mass-transport phenomena in proton-exchange membrane fuel-cells using O_2/He, O_2/Ar and O_2/N_2 mixtures. 1. Experimental-analysis. *J Electrochem Soc*. 1994;141:2084–2088.
41. Feser JP, Prasad AK, Advani SG. Experimental characterization of in-plane permeability of gas diffusion layers. *J Power Sources*. 2006;162:1226–1231.
42. Jiang RC, Kunz HR, Fenton JM. Influence of temperature and relative humidity on performance and CO tolerance of PEM fuel cells with Nafion (R)-Teflon (R)-Zr(HPO4)(2). *Electrochimica Acta*. 2006;51:5596–5605.
43. Williams MV, Begg E, Bonville L, Kunz HR, Fenton JM. Characterization of gas diffusion layers for PEMFC. *J Electrochem Soc*. 2004;151:A1173–A1180.
44. Williams MV, Kunz HR, Fenton JM. Analysis of polarization curves to evaluate polarization sources in hydrogen/air PEM fuel cells. *J Electrochem Soc*. 2005;152:A635–A644.
45. Kulikovsky AA. Optimal shape of catalyst loading across the active layer of a fuel cell. *Electrochem Commun*. 2009;11:1951–1955.
46. Kulikovsky AA. Resistive spot in a fuel cell stack: exact solutions. *J Fuel Cell Sci Technol*. 2009;6(1):011024.
47. Kulikovsky AA. Optimal effective diffusion coefficient of oxygen in the cathode catalyst layer of polymer electrode membrane fuel cells. *Electrochem Solid State Lett*. 2009;12:B53–B56.
48. Lee HK, Park JH, Kim DY, Lee TH. A study on the characteristics of the diffusion layer thickness and porosity of the PEMFC. *J Power Sources*. 2004;131:200–206.
49. Passalacqua E, Squadrito G, Lufrano F, Patti A, Giorgi L. Effects of the diffusion layer characteristics on the performance of polymer electrolyte fuel cell electrodes. *J Appl Electrochem*. 2001;31:449–454.
50. Jang JH, Yan WM, Shih CC. Numerical study of reactant gas transport phenomena and cell performance of proton exchange membrane fuel cells. *J Power Sources*. 2006;156:244–252.
51. Weber AZ. Effective diffusion-medium thickness for simplified polymer-electrolyte-fuel-cell modeling. *Electrochimica Acta*. 2008; 54:311–315.
52. Natarajan D, Van Nguyen T. Current distribution in PEM fuel cells. Part 1: oxygen and fuel flow rate effects. *AICHE J*. 2005;51:2587–2598.
53. Yi JS, Nguyen TV. An along-the-channel model for proton exchange membrane fuel cells. *J Electrochem Soc*. 1998;145:1149–1159.
54. Wang XD, Huang YX, Cheng CH, Jang JY, Lee DJ, Yan WM, Su A. Flow field optimization for proton exchange membrane fuel cells with varying channel heights and widths. *Electrochimica Acta*. 2009;54: 5522–5530.
55. Williams MV, Kunz HR, Fenton JM. Influence of convection through gas-diffusion layers on limiting current in PEM FCs using a serpentine flow field. *J Electrochem Soc*. 2004;151:A1617–A1627.
56. Yan WM, Chen CY, Mei SC, Soong CY, Chen FL. Effects of operating conditions on cell performance of PEM fuel cells with conventional or interdigitated flow field. *J Power Sources*. 2006;162:1157–1164.
57. Yan WM, Mei SC, Soong CY, Liu ZS, Song DT. Experimental study on the performance of PEM fuel cells with interdigitated flow channels. *J Power Sources*. 2006;160:116–122.
58. Abdulla A, Laney K, Padilla M, Sundaresan S, Benziger J. Efficiency of hydrogen recovery from reformate with a polymer electrolyte hydrogen pump. *AIChE J*. DOI: 10.1002/aic.12406.

Manuscript received Apr. 6, 2010, revision received Aug. 6, 2010, and final revision received Sept. 27, 2010.